Opportunity Detection for OFDMA-Based Cognitive Radio Systems with Timing Misalignment

Mustafa E. Şahin, Ismail Guvenc, *Member, IEEE*,
and Hüseyin Arslan, *Senior Member, IEEE*

***Abstract*— Accurate detection of spectrum opportunities within the frequency band of an orthogonal frequency division multiple access (OFDMA) system carries critical importance for OFDMA-based cognitive radios. In this paper, we analyze the opportunity detection performances of energy detection and ESPRIT (estimation of signal parameters by rotational invariance techniques) algorithms in the presence of timing misalignments in uplink (UL) OFDMA. For the energy detector, the statistics of subcarrier power are derived considering timing misalignments, and they are verified through computer simulations. Using these statistics, which take inter-carrier-interference (ICI) effects into account, receiver operating characteristics (ROCs) of the energy detector receiver are obtained. It is shown that energy detection has a considerably better performance than ESPRIT, especially when the subcarrier assignment changes frequently. Moreover, a closed form expression is derived for the UL-OFDMA synchronization point that minimizes the ICI. Finally, it is shown that employing resource allocation blocks with larger sizes in the primary network yields better opportunities for the cognitive radio.**

***Index Terms*— Cognitive radio, Energy Detector, ESPRIT, Femtocell, ICI, OFDMA, Opportunity Detection, Receiver Operating Characteristics, OFDM Synchronization, Spectrum Sensing, Timing Misalignment.**

I. Introduction

The growing number of wireless technologies may force future systems to share the same spectrum. Cognitive radio [1] is seen as a promising approach in this direction [2], [3]. Cognitive radio introduces the concept of opportunistic spectrum usage [4] in which a secondary network utilizes unused parts of a spectrum that is owned by a primary system. Cognitive radios are required to reliably sense the spectrum opportunities in order to minimize probability of false alarms (PFA) and probability of missed detections (PMD) [5], [6].

For an orthogonal frequency division multiple access (OFDMA) based cognitive radio, spectrum opportunity can be defined as the set of subcarriers that are not utilized by the primary system. A threshold based detector such as in [7] can be employed for detecting the spectrum opportunities, where appropriate selection of the threshold is critical for a good detection performance. Spectrum sensing performance of energy detectors can be quantified by receiver operating characteristic (ROC) curves (see e.g. [8]). A particularly challenging scenario that has not been considered in detail in the prior art for cognitive radio systems is when some of the uplink (UL) OFDMA user signals arrive at the receiver with delays larger than the CP of the symbol (see e.g., [9]-[11], and Fig. 1). For example, in Fig. 1(b), the secondary user SU-1 communicates with SU-2 utilizing the available spectrum opportunities. However, the signals of the primary users arriving at SU-2 after the CP of SU-1 (i.e., UL signals of mobile stations MS-1 and MS-4) result in inter-symbol interference (ISI) as well as inter-carrier interference (ICI), which may considerably decrease the spectrum opportunities.

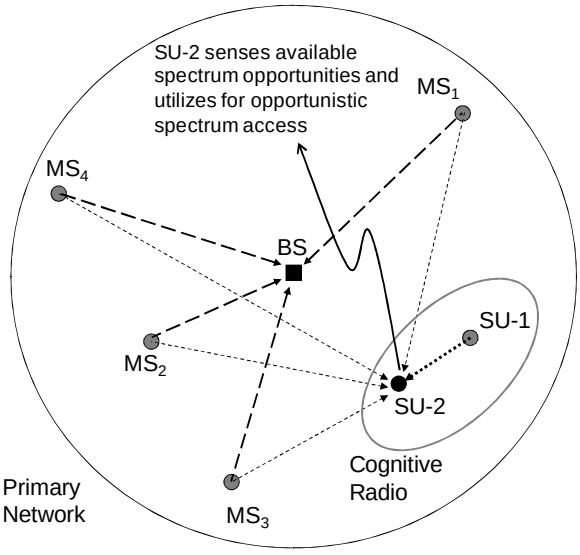

(a) Cognitive radio scenario in consideration.

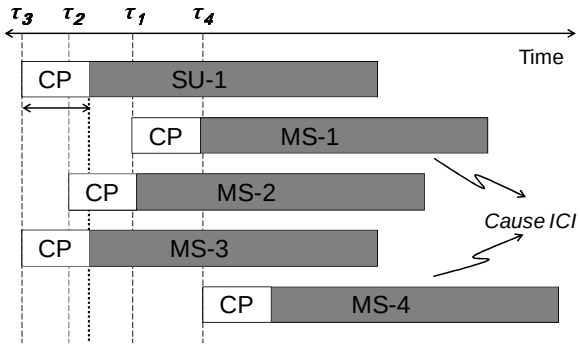

(b) The primary network and cognitive radio signals arriving at SU-2 and the timing misalignment problem.

Fig. 1. Cognitive radio scenario in consideration and illustration of the timing misalignment problem due to users' signals arriving after the CP of SU-1.

This paper was presented in part at the IEEE Global Communications Conference (GLOBECOM), New Orleans, LA, November 2008.

M. E. Şahin and H. Arslan are with the Electrical Engineering Department, University of South Florida, Tampa, FL 33613 USA (e-mail: msahin@mail.usf.edu; arslan@eng.usf.edu)

I. Guvenc is with DOCOMO Communications Laboratories USA, Inc., Palo Alto, CA 94304 USA (e-mail: iguvenc@docomolabs-usa.com).

An interesting case where such a timing misalignment problem may occur is the coexistence of a femtocell network [12], [13] with a macrocell network, both of which employ OFDMA. As discussed in [14] and [15], macrocell and femtocell may coexist through either a split-spectrum approach, where both networks are assigned orthogonal bands, or a shared-spectrum approach, where unused parts of the macrocell spectrum are utilized by the femtocell that acts as a cognitive radio. In a shared-spectrum scenario, while the macrocell users are synchronized with the macrocell base station (BS) through initial/periodic ranging [16], [17], their signals may arrive at the femtocell BS with different delays (see [18] for an analysis of arrival times at the femtocell BS), which can make detection of spectrum opportunities by the femtocell quite challenging.

In this paper, detection of spectrum opportunities in UL-OFDMA is investigated in the presence of considerable timing misalignment between users (see e.g. [19]). Taking into account the effects of ICI that appear as a result of timing misalignments, the statistics of the energy detector receiver are obtained, and the related ROCs for spectrum sensing are derived. Moreover, a closed form expression for the primary user distance that causes the strongest interference to the cognitive radio is obtained. Finally, optimum UL-OFDMA synchronization point that minimizes the interference to the cognitive radio is calculated[1]. Through computer simulations, opportunity detection error probabilities using the energy detector are determined for various scenarios and they are compared with the detection performance of the estimation of signal parameters by rotational invariance techniques (ESPRIT) algorithm. Impact of the primary network's resource allocation block size on the cognitive radio is also investigated using the parameters specified in LTE and WiMAX standards.

Organization of this paper is as follows. Section II provides the system model, while Section III shortly introduces energy detection based and ESPRIT algorithm based spectrum sensing approaches. In Section IV, the statistics of the energy detector decision variable are investigated, and the user distance yielding the highest interference is derived. In Section V, ROCs with and without timing misalignment are derived for receivers that employ noise-based threshold and normalized threshold. Section VI investigates the optimum synchronization point for an UL-OFDMA receiver, Section VII presents the simulation results, and Section VIII concludes the paper.

II. UL-OFDMA System Model

Consider an OFDMA system with $N_{\rm u}$ users in the uplink. The sampled time domain signal at the transmitter of user i can be written as

$$x_i^{(m)}(n) = \sqrt{P_{{\rm tx},i}} \sum_{k\in\mathbf{\Gamma}_i} X_i^{(m)}(k) e^{\frac{j2\pi kn}{N}}\ , -N_{\rm cp} \le n \le N-1, \tag{1}$$

where m is the symbol index, $P_{{\rm tx},i}$ is the transmit power for user i, $k \in \mathbf{\Gamma}_i$ is the subcarrier index, $\mathbf{\Gamma}_i$ is the set of subcarriers of length N_i assigned to user i out of N total subcarriers, $N_{\rm cp}$ is the length of the cyclic prefix, and $X_i^{(m)}(k)$ is the data on the kth subcarrier and mth symbol of the ith user.

The time domain aggregate received signal is the superposition of signals from all users, each of which propagates through a different multipath channel and arrives at the receiver with a delay $\tilde{\delta}_i = \lceil N\tilde{\tau}_i/T \rceil$, where $\tilde{\tau}_i$ is the propagation delay experienced by user i, and T is the duration of the useful part of the symbol. Then, aggregate discrete-time received signal can be expressed as

$$y(n) = \sum_{i=1}^{N_{\rm u}} y_i(n) + w(n), \tag{2}$$

where $w(n)$ denotes the additive white Gaussian noise (AWGN), and

$$y_i(n) = \sqrt{P_{{\rm rx},i}} \sum_{l=0}^{L-1} \alpha_i^{(m)}(l) \times \sum_{m=-\infty}^{\infty} x_i^{(m)}\Big(n - D_{l,i} - m(N+N_{\rm cp})\Big), \tag{3}$$

where $P_{{\rm rx},i}$ is the received power for user i, L denotes the total number of multipath components (MPCs), $\alpha_i^{(m)}(l)$ is the lth MPC for user i, and $D_{l,i} = \lceil N\tau_{l,i}/T \rceil + \tilde{\delta}_i$, where $\tau_{l,i}$ is the delay of the lth MPC for user i.

If $D_{l,i} \le N_{\rm cp}$, it is easy to prove that the frequency domain signal for the kth subcarrier of user i is given by

$$Y_i^{(m)}(k) = \sqrt{E_{{\rm sc},i}} X_i^{(m)}(k) \sum_{l=0}^{L-1} \alpha_i^{(m)}(l) e^{-\frac{j2\pi kD_{l,i}}{N}}\ , \tag{4}$$

where $E_{{\rm sc},i}$ is the average received energy per subcarrier for user i, which is equal to $P_{{\rm rx},i}$. On the other hand, if $D_{l,i} > N_{\rm cp}$, the FFT window at the receiver will include signals from two consecutive symbols of the transmitted signal. As a consequence, this will result in inter-symbol interference as well as inter-carrier interference. Getting the FFT of (3), the received signal on the kth subcarrier of user i can be written as [11]

$$Y_i^{(m)}(k) = \frac{\sqrt{E_{{\rm sc},i}}}{N} \sum_{l=1}^{L} \alpha_i^{(m)}(l) \times \left\{ \sum_{n=0}^{D_{l,i}-N_{\rm cp}-1} x_i^{(m-1)}(n+N+N_{\rm cp}-D_{l,i}) e^{-\frac{j2\pi kn}{N}} + \sum_{n=D_{l,i-N_{\rm cp}}}^{N-1} x_i^{(m)}(n-D_{l,i}) e^{-\frac{j2\pi kn}{N}} \right\}. \tag{5}$$

After plugging (1) into (5) and some manipulation, we have

$$Y_i^{(m)}(k) = \sqrt{E_{{\rm sc},i}} \sum_{l=0}^{L-1} \alpha_i^{(m)}(l) \times \Big\{ S_{{\rm d},i,l}(k) + I_{1,i,l}(k) + I_{2,i,l}(k) \Big\}, \tag{6}$$

[1]Note that UL-OFDMA synchronization has been investigated in several works in the prior art (see e.g. [20] and [21] and the references therein). In this paper, we look at the timing synchronization problem from a secondary system's perspective for minimizing interference, which has not been considered in the literature to the best of our knowledge.

where the desired signal, interference from the same subcarrier of the previous symbol, and the total interference from other subcarriers are respectively given as

$$S_{\mathrm{d},i,l}(k) = X_i^{(m)}(k) K_{1,i,l}(k) e^{\frac{-j2\pi k D_{l,i}}{N}} \tag{7}$$

$$I_{1,i,l}(k) = X_i^{(m-1)}(k) K_{2,i,l}(k) e^{\frac{-j2\pi k (D_{l,i}-N_{\mathrm{cp}})}{N}} \tag{8}$$

$$I_{2,i,l}(k) = \frac{1}{N} \sum_{\substack{p\in\mathbf{\Gamma}_i \\ p\neq k}} \underbrace{\left[\frac{1-e^{\frac{j2\pi(p-k)(D_{l,i}-N_{\mathrm{cp}})}{N}}}{1-e^{\frac{j2\pi(p-k)}{N}}}\right]}_{h_i(p,k)} \times \underbrace{\left(-X_i^{(m)}(p) e^{-\frac{j2\pi p D_{l,i}}{N}} + X_i^{(m-1)}(p) e^{\frac{j2\pi p (N_{\mathrm{cp}}-D_{l,i})}{N}}\right)}_{g_i(p)}, \tag{9}$$

where

$$K_{1,i,l}(k) = \frac{N - D_{l,i} + N_{\mathrm{cp}}}{N} \times \mathcal{I}(i,k) \ , \qquad K_{2,i,l}(k) = \frac{D_{l,i} - N_{\mathrm{cp}}}{N} \times \mathcal{I}(i,k), \tag{10}$$

with $\mathcal{I}(i,k)$ denoting an indicator function given by

$$\mathcal{I}(i,k) = \begin{cases} 1 \ , & \text{if } k \in \mathbf{\Gamma}_i \ , \\ 0 \ , & \text{if } k \notin \mathbf{\Gamma}_i \ . \end{cases} \tag{11}$$

Note that the interference terms $I_{1,i,l}(k)$ and $I_{2,i,l}(k)$ will both be zero if the received MPC is located within the CP duration. The aggregate frequency-domain signal can then be written as

$$Y^{(m)}(k) = \sum_{i=1}^{N_{\mathrm{u}}} Y_i^{(m)}(k) + W(k) \ , \tag{12}$$

where $W(k) \sim \mathcal{CN}\big(0, \sigma^2\big)$ is the DFT of $w(n)$, $\sigma^2 = N_0/2$, and $\mathcal{CN}\big(\mu, \sigma^2\big)$ denotes the distribution of a circularly symmetric complex Gaussian random variable with mean μ and variance σ^2.

III. Spectrum Sensing Techniques

Different methods may be considered for the detection of spectrum opportunities in an OFDMA system. In this paper, energy detection and ESPRIT algorithms are considered. Moreover, impact of subcarrier assignment strategy on the opportunity detection performance is evaluated.

A. Energy Detector Method

In the energy detector method, based on (6), we consider the following decision variable and compare it with a threshold ξ

$$P^{(m)}(k) = \left|Y^{(m)}(k)\right|^2 \underset{H_0}{\overset{H_1}{\gtrless}} \xi \ , \tag{13}$$

where hypothesis H_1 implies that subcarrier k is occupied, and hypothesis H_0 implies that it is not. A diagram of the energy detector method is provided in Fig. 2. Statistics of the decision variable $P^{(m)}(k)$ in the presence of timing misalignment will be discussed in more detail in Section IV, while possible approaches for selecting the threshold ξ are discussed in Section V.

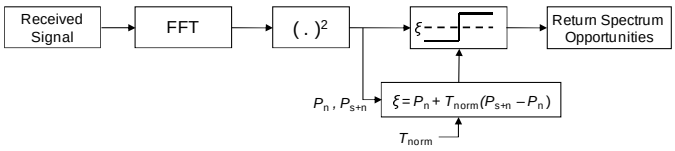

Fig. 2. Diagram of the energy detector method.

B. ESPRIT Method

ESPRIT is a high resolution signal parameter estimation algorithm that exploits the shift invariance property of signals [22]. It belongs to the class of signal subspace methods in that it relies on an eigendecomposition of the covariance matrix of the received signal [23]. The algorithm has been employed in a wide variety of applications including direction-of-arrival estimation in antenna arrays [22], channel estimation in multipath fading channels [24], and estimating the parameters of sinusoids in noise [25].

The problem of determining the occupied subcarriers in an OFDMA signal can be considered as identifying the number and frequencies of a set of sinusoids in additive noise. OFDM based signals are suitable for implementing ESPRIT because they are made shift invariant by the addition of a cyclic prefix, which means that a time shift not exceeding the CP does not alter the statistical features of the OFDM signal. Exploiting this property of the OFDM signal, carrier frequency offset estimation using ESPRIT was performed in [26]. In [27], ESPRIT algorithm was proposed for estimating the occupied subcarriers of an OFDM symbol. Although it is known that ESPRIT cannot be the optimum detection method when the maximum delay observed in the system is larger than the CP (due to the degradation in the shift invariance of OFDM symbols), in this paper, the ESPRIT performance in an asynchronous UL-OFDMA system is simulated to provide a relative measure for the energy detection performance.

In the practical ESPRIT implementation for determining the occupied subcarriers of an OFDM symbol, the first step is to estimate the number of occupied subcarriers (N_{ocp}), which is done via the minimum descriptive length (MDL) algorithm introduced in [28]. Estimation of subcarrier frequencies, on the other hand, is performed by constructing the auto- and cross-covariance matrices of the received signal. From the received signal $y(n)$, two sample vectors $\boldsymbol{y}(n)$ and $\boldsymbol{z}(n)$ of length Υ are formed

$$\begin{aligned} \boldsymbol{y}(n) &= [y(n),\, y(n+1),\, \cdots,\, y(n+\Upsilon-1)], \\ \boldsymbol{z}(n) &= [y(n+1),\, y(n+2),\, \cdots,\, y(n+\Upsilon)], \end{aligned} \tag{14}$$

where Υ is equal to $\mathcal{M} \times (N + N_{\mathrm{cp}})$, $\mathcal{M}$ being the number of adjacent symbols with the same occupied subcarriers.

The auto-covariance matrix $\mathbf{R}_{\mathrm{yy}}$ and cross-covariance matrix $\mathbf{R}_{\mathrm{yz}}$ are obtained as follows

$$\mathbf{R}_{\mathrm{yy}} = \mathrm{E}\{\boldsymbol{y}(n)\boldsymbol{y}^*(n)\}, \text{ and } \mathbf{R}_{\mathrm{yz}} = \mathrm{E}\{\boldsymbol{y}(n)\boldsymbol{z}^*(n)\}, \tag{15}$$

where $E\{\cdot\}$ denotes the expectation operation. It is important to note that the reliability of $\mathbf{R}_{\mathrm{yy}}$ and $\mathbf{R}_{\mathrm{yz}}$ is directly proportional to $\mathcal{M}$. By performing an eigen-decomposition on $\mathbf{R}_{\mathrm{yy}}$, its eigenvalues are determined, where the minimum eigenvalue

λ_{min} is the noise variance[2]. Noise power is subtracted from $\mathbf{R}_{\rm yy}$ and $\mathbf{R}_{\rm yz}$ to obtain

$$\mathbf{C}_{\rm yy} = \mathbf{R}_{\rm yy} - \lambda_{min}\mathbf{I} \text{ and } \mathbf{C}_{\rm yz} = \mathbf{R}_{\rm yz} - \lambda_{min}\mathbf{Z}, \quad (16)$$

where $\mathbf{I}$ is the identity matrix, and $\mathbf{Z}$ is a matrix with ones on the first subdiagonal and zeros elsewhere. The frequencies of the occupied subcarriers are yielded by the first $N_{\rm ocp}$ largest generalized eigenvalues of the matrix pair $(\mathbf{C}_{\rm yy}, \mathbf{C}_{\rm yz})$ (The reader is referred to [25] for a step-by-step guide of the ESPRIT algorithm).

The matrix operations that it requires make the ESPRIT algorithm highly computationally complex and may induce an extended processing delay. This kind of a delay renders ESPRIT less feasible in a real-time application.

IV. Statistics of the Energy Detector Decision Variable with Timing Misalignment

In order to analyze how the timing misalignment problem affects the opportunity detection, the statistics of the decision variable in (13) have to be evaluated. After plugging (12) into (13), we have

$$\begin{aligned} P^{(m)}(k) = \left|Y^{(m)}(k)\right|^2 &= \sum_{i=1}^{N_{\rm u}} \left|Y_i^{(m)}(k)\right|^2 + |W(k)|^2 \\ &+ 2{\rm Re}\Big\{ \underbrace{W^*(k)\sum_{i=1}^{N_{\rm u}} Y_i^{(m)}(k)}_{\rm Zero-mean\ RV} \Big\} \\ &+ 2\sum_{i=1}^{N_{\rm u}-1}\sum_{j=i+1}^{N_{\rm u}} Y_i^{*(m)}(k) Y_j^{(m)}(k), \end{aligned} \quad (17)$$

where the last term of (17) is 0 since $Y_i^{(m)}(k)$ and $Y_j^{(m)}(k)$ cannot be non-zero simultaneously. The statistics of (17) can be evaluated by analyzing the statistics of the individual terms as will be discussed below. To keep the expressions analytically tractable[3], we consider $L = 1$ in (6), and drop the multipath indices from related expressions in (6)-(9).

First, using (4), we may write $\left|Y_i^{(m)}(k)\right|^2$ as

$$\begin{aligned} \left|Y_i^{(m)}(k)\right|^2 &= E_{{\rm sc},i}\left|S_{{\rm d},i}(k) + I_{1,i}(k) + I_{2,i}(k)\right|^2 \\ &= E_{{\rm sc},i}\Big[\left|S_{{\rm d},i}(k)\right|^2 + \left|I_{1,i}(k)\right|^2 + \left|I_{2,i}(k)\right|^2 \\ &+ 2{\rm Re}\Big\{ S_{{\rm d},i}^*(k)I_{1,i}(k) + S_{{\rm d},i}^*(k)I_{2,i}(k) + I_{1,i}^*(k)I_{2,i}(k) \Big\}\Big], \end{aligned} \quad (18)$$

where

$$\left|S_{{\rm d},i}(k)\right|^2 = \left|X_i^{(m)}(k)\right|^2 K_{1,i}^2(k), \quad (19)$$

$$\left|I_{1,i}(k)\right|^2 = \left|X_i^{(m-1)}(k)\right|^2 K_{2,i}^2(k), \quad (20)$$

$$\begin{aligned} \left|I_{2,i}(k)\right|^2 = \frac{1}{N^2}\Big(&\sum_{\substack{p\in\mathbf{\Gamma}_i \\ p\neq k}} \left|h_i^2(p,k)\right|\left|g_i^2(p)\right| \\ &+ \underbrace{{\rm Re}\Big\{ \sum_{\substack{p\in\mathbf{\Gamma}_i \\ p\neq k}} \sum_{\substack{q\in\mathbf{\Gamma}_i \\ q\neq k, q\neq p}} h_i^*(p,k)h_i(q,k)g_i^*(p)g_i(q) \Big\}}_{\rm Zero-mean\ RV} \Big), \end{aligned} \quad (21)$$

$$S_{{\rm d},i}^*(k)I_{1,i}(k) = X_i^{*(m)}(k)X_i^{(m-1)}(k)K_{1,i}(k)K_{2,i}(k)e^{\frac{j2\pi kN_{\rm cp}}{N}}, \quad (22)$$

$$\begin{aligned} S_{{\rm d},i}^*(k)I_{2,i}(k) = &\frac{1}{N}X_i^{*(m)}(k)K_{1,i}(k)e^{\frac{j2\pi kD_{l,i}}{N}} \\ &\times \sum_{\substack{p\in\mathbf{\Gamma}_i \\ p\neq k}} h_i(p,k)g_i(p), \end{aligned} \quad (23)$$

$$\begin{aligned} I_{1,i}^*(k)I_{2,i}(k) = &\frac{1}{N}X_i^{*(m-1)}(k)K_{2,i}(k)e^{\frac{j2\pi k(D_{l,i}-N_{\rm cp})}{N}} \\ &\times \sum_{\substack{p\in\mathbf{\Gamma}_i \\ p\neq k}} h_i(p,k)g_i(p)\ , \end{aligned} \quad (24)$$

with, as indicated in (9),

$$g_i(p) = -X_i^{(m)}(p)e^{-\frac{j2\pi pD_{l,i}}{N}} + X_i^{(m-1)}(p)e^{\frac{j2\pi p(N_{\rm cp}-D_{l,i})}{N}}, \quad (25)$$

$$\begin{aligned} h_i(p,k) &= \frac{1-e^{\frac{j2\pi(p-k)(D_{l,i}-N_{\rm cp})}{N}}}{1-e^{\frac{j2\pi(p-k)}{N}}}\ , \\ h_i^2(p,k) &= \frac{1-\cos\Big(\frac{2\pi(p-k)(D_{l,i}-N_{\rm cp})}{N}\Big)}{1-\cos\Big(\frac{2\pi(p-k)}{N}\Big)}\ . \end{aligned} \quad (26)$$

Note that (22)-(24) as well as the indicated terms in (17) and (21) are zero-mean random-variables (RVs). Then, the mean of (17) can be evaluated as

$${\rm E}\Big\{P^{(m)}(k)\Big\} = \sum_{i=1}^{N_{\rm u}} {\rm E}\Big\{\left|Y_i^{(m)}(k)\right|^2\Big\} + n_{\rm d}\sigma^2\ , \quad (27)$$

where $n_{\rm d}$ denotes the degree of freedom (DOF) of noise terms, and calculation of ${\rm E}\Big\{\left|Y_i^{(m)}(k)\right|^2\Big\}$ will be discussed in Appendix A.

On the other hand, the variance of (17) is

$$\begin{aligned} {\rm Var}\Big\{P^{(m)}(k)\Big\} = &\sum_{i=1}^{N_{\rm u}} {\rm Var}\Big\{\left|Y_i^{(m)}(k)\right|^2\Big\} + 2n_{\rm d}\sigma^4 \\ &+ 8n_{\rm d}\sigma^4\sum_{i=1}^{N_{\rm u}} {\rm E}\Big\{\left|Y_i^{(m)}(k)\right|^2\Big\}\ , \end{aligned} \quad (28)$$

[2]Note that since $\Upsilon > N_{\rm ocp}$, $\mathbf{R}_{\rm yy}$ is a singular matrix; hence, $\Upsilon - N_{\rm ocp}$ of its smaller eigenvalues yield the noise variance.

[3]For the derivation of the statistics of (17) in a multipath channel, the reader is referred to Appendix-B.

where calculation of the variances of the first two terms are straight-forward, and the variance of the third term is calculated as

$$\begin{aligned}&\mathrm{Var}\Big\{2\mathrm{Re}\Big\{W^*(k)\sum_{i=1}^{N_\mathrm{u}}Y_i^{(m)}(k)\Big\}\Big\}\\&=\mathrm{E}\Big\{4W^2(k)\Big(\sum_{i=1}^{N_\mathrm{u}}\big|Y_i^{(m)}(k)\big|^2\\&\qquad+\sum_{i=1}^{N_\mathrm{u}-1}\sum_{j=i}^{N_\mathrm{u}}Y_i^{*(m)}(k)Y_j^{(m)}(k)\Big)\Big\} \quad (29)\\&=8n_\mathrm{d}\sigma^4\sum_{i=1}^{N_\mathrm{u}}\mathrm{E}\Big\{\Big|Y_i^{(m)}(k)\Big|^2\Big\}\ . \quad (30)\end{aligned}$$

Hence, calculation of $\mathrm{E}\Big\{\Big|Y_i^{(m)}(k)\Big|^2\Big\}$ and $\mathrm{Var}\Big\{\Big|Y_i^{(m)}(k)\Big|^2\Big\}$ are sufficient for obtaining the statistics of (17) as in (27) and (28), as will be illustrated for different modulation schemes in Appendix A.

A. User Distance Yielding the Strongest Interference

The ICI power from a certain user is scaled by the received signal energy from that user, $E_{\mathrm{sc},i}$, as indicated in (15). However, in (15), the distance-dependency of the received signal energies was not explicitly taken into account, and it was assumed that $E_{\mathrm{sc},i}$ is a given parameter. However, in practice, both the received signal's delay and energy depend on the distance between the user and the secondary receiver.

Assuming a single tap channel, user delays are directly proportional to the user distances (d_i) through $D_{1,i}=\frac{d_i}{cT_s}$, where c is the speed of light, and T_s is the sampling time. Moreover, $E_{\mathrm{sc},i}$ also depends on d_i through $E_{\mathrm{sc},i}=\frac{\lambda^2}{(4\pi)^2 d_i^\gamma}P_\mathrm{tx}$, where λ is the wavelength of the transmitted signal, and γ is the path loss coefficient. Since the impacts of d_i on $D_{1,i}$ and $E_{\mathrm{sc},i}$ are inversely proportional to each other[4], it is expected that the interference power will be maximized at a certain distance and then will start decreasing with d_i. Determining the d_i that causes the strongest interference might be useful for certain practical applications. An example can be a femtocell that has access to the subcarrier allocation map of the macrocell network as well as to the locations of the macrocell users (through its backbone connection to the macrocell network). If the femtocell knows that users that are located at/around a specific distance cause the highest interference, it can avoid using the empty subcarriers that are adjacent to these users' subcarriers. Therefore, we analytically derived a closed-from expression for the user distance that causes the strongest interference.

Through simulations, it is determined that $\sum_{k\neq p}I_{1,i}^2(k)$ is negligible compared to $\sum_{k\neq p}I_{2,i}^2(k)$. Hence, the derivation is based on finding the distance where $I_{2,i}^2(k)$ (ICI) is maximized. The total interference power that is caused by a certain subcarrier p, summed over all empty subcarriers, is given by

$$\sum_{k\neq p}I_{2,i}^2(k)=\frac{\lambda^2}{(4\pi)^2 d_i^2}\frac{2}{N^2}\sum_{k\neq p}h_i^2(p,k)\ , \quad (31)$$

Replacing d_i with $cD_{1,i}T_s$, (31) can be rewritten as

$$\sum_{k\neq p}I_{2,i}^2(k)=\frac{2}{\big(4\pi fNT_sD_{1,i}\big)^2}\sum_{k\neq p}h_i^2(p,k)\ , \quad (32)$$

where f is the carrier frequency of the system. Differentiating (32) with respect to $D_{1,i}$ one obtains

$$\begin{aligned}&\frac{d\sum_{k\neq p}I_{2,i}^2(k)}{dD_{1,i}}=\frac{2}{\big(4\pi fNT_s\big)^2}\\&\times\Bigg(-\frac{2}{D_{1,i}^3}\sum_{k\neq p}\frac{1-\cos\Big(\frac{2\pi(p-k)(D_{1,i}-N_\mathrm{cp})}{N}\Big)}{1-\cos\Big(\frac{2\pi(p-k)}{N}\Big)}\\&\quad+\frac{1}{D_{1,i}^2}\sum_{k\neq p}\frac{\sin\Big(\frac{2\pi(p-k)(D_{1,i}-N_\mathrm{cp})}{N}\Big)}{1-\cos\Big(\frac{2\pi(p-k)}{N}\Big)}\frac{2\pi(p-k)}{N}\Bigg). \quad (33)\end{aligned}$$

The point where the ICI power is maximum can be found by equating (33) to 0, which yields

$$\begin{aligned}&\frac{2}{D_{1,i}}\sum_{k\neq p}\frac{1-\cos\Big(\frac{2\pi(p-k)(D_{1,i}-N_\mathrm{cp})}{N}\Big)}{1-\cos\Big(\frac{2\pi(p-k)}{N}\Big)}\\&=\sum_{k\neq p}\frac{\sin\Big(\frac{2\pi(p-k)(D_{1,i}-N_\mathrm{cp})}{N}\Big)}{1-\cos\Big(\frac{2\pi(p-k)}{N}\Big)}\frac{2\pi(p-k)}{N}\ . \quad (34)\end{aligned}$$

The trigonometric terms in (34) can be approximated using Taylor series expansion under the condition that the inputs of $\cos(x)$ and $\sin(x)$ satisfy $-1<x<1$. Although this condition is met only for very small values of $(p-k)$, approximation is still useful since ICI is not significant for large values of $(p-k)$. Substituting the sine and cosine functions in (34) with the first two terms of their Taylor expansion, i.e. $\cos(x)\approx 1-\frac{x^2}{2}$ and $\sin(x)\approx x-\frac{x^3}{3!}$, one obtains

$$\begin{aligned}&\sum_{\substack{k=p-a\\k\neq p}}^{k=p+a}\frac{\big(D_{1,i}-N_\mathrm{cp}\big)^2}{D_{1,i}}\\&=\sum_{\substack{k=p-a\\k\neq p}}^{k=p+a}\Bigg(\big(D_{1,i}-N_\mathrm{cp}\big)-\frac{1}{6}\Big(\frac{2\pi(p-k)}{N}\Big)^2\big(D_{1,i}-N_\mathrm{cp}\big)^3\Bigg).\end{aligned} \quad (35)$$

where a is a small value that enables Taylor approximation and needs to be set inversely proportional with N_cp. Empirically, it is found that $\frac{N}{2N_\mathrm{cp}}$ is an appropriate value for a. Utilizing summation formulas, one obtains

$$\begin{aligned}&2a\frac{D_{1,i}-N_\mathrm{cp}}{D_{1,i}}\\&\quad=2a-\frac{1}{6}\Big(\frac{2\pi\big(D_{1,i}-N_\mathrm{cp}\big)}{N}\Big)^2\frac{a(a+1)(2a+1)}{3}\ , \quad (36)\end{aligned}$$

[4] $D_{1,i}$ increases linearly with d_i, and $E_{\mathrm{sc},i}$ decreases with γth power of d_i.

which, after some manipulations, leads to

$$D_{1,i}^3 - 2N_{\rm cp}D_{1,i}^2 + N_{\rm cp}^2 D_{1,i} - \frac{36N_{\rm cp}}{\left(\frac{2\pi}{N}\right)^2(a+1)(2a+1)} = 0 \ . \tag{37}$$

Note that two roots of (37) constitute a complex conjugate pair, and the third root is a real number, which yields the d_i causing the highest ICI. As it will be verified in Section VII, it is found that a quite accurate approximation for $D_{1,i}$ that yields the highest interference is $2N_{\rm cp}$.

V. Receiver Operating Characteristics

For the detection of occupied subcarriers, we consider two types of threshold-based techniques for selecting ξ in (13) in this paper: noise-based threshold (NBT) and normalized threshold (NT). While the threshold using the first approach is set based only on the noise level, the threshold using the second approach scales with the total received signal energy.

A. Noise-based threshold

If the noise variance σ^2 is known, the threshold that satisfies a certain PFA can be selected. When a subcarrier k is not occupied by any user, (13) follows a centralized Chi-square distribution, whose cumulative distribution function (CDF) is given by [29]

$$\mathrm{F}_Y(y) = 1 - e^{-y/2\sigma^2}\sum_{\kappa=0}^{M-1}\frac{1}{\kappa!}\left(\frac{y}{2\sigma^2}\right)^{\kappa} \ , \tag{38}$$

where $M = n_{\rm d}/2$ is an integer. For complex noise, we have $n_{\rm d} = 2$, and (38) becomes the CDF of an exponential distribution. Then, the PFA for a certain threshold ξ as in (13) becomes

$$\mathrm{P}_{\rm fa}(\xi) = 1 - \mathrm{F}_Y(\xi) = e^{-\xi/2\sigma^2} \ , \tag{39}$$

where the threshold may also be written in terms of the PFA as

$$\xi = \mathrm{F}_Y^{-1}\big(1 - \mathrm{P}_{\rm fa}\big) \ . \tag{40}$$

When subcarrier k is occupied, on the other hand, (13) follows a non-centralized Chi-square distribution, whose CDF is given by [29]

$$\tilde{\mathrm{F}}_Y(y, E_{{\rm sc},i}) = 1 - Q_M\left(\frac{\sqrt{E_{{\rm sc},i}}}{\sigma}, \frac{\sqrt{y}}{\sigma}\right) \ , \tag{41}$$

where $Q_M(a,b)$ is the Marcum-Q function given by

$$Q_M(a,b) = \int_b^{\infty} x\left(\frac{x}{a}\right)^{M-1} e^{-(x^2+a^2)/2} I_{M-1}(ax)\mathrm{d}x \ , \tag{42}$$

with $I_\zeta(x)$ denoting the ζth order modified Bessel function of the first kind [29]. Then, using (39), probability of detection $\mathrm{P}_{\rm d}$ corresponding to a certain $\mathrm{P}_{\rm fa}$ becomes

$$\begin{aligned}\mathrm{P}_{\rm d}(\mathrm{P}_{\rm fa}) &= 1 - \tilde{\mathrm{F}}_Y(\xi, E_{{\rm sc},i}) \\ &= Q_M\left(\frac{\sqrt{E_{{\rm sc},i}}}{\sigma}, \frac{\sqrt{\mathrm{F}_Y^{-1}\big(1-\mathrm{P}_{\rm fa}\big)}}{\sigma}\right) \ .\end{aligned} \tag{43}$$

The relationship in (43) that relates the $\mathrm{P}_{\rm d}$ to $\mathrm{P}_{\rm fa}$ is commonly referred as the receiver operating characteristic curves.

In the presence of ICI, since the statistics of the received power will change, the ROC performance will get worse. In particular, using again the Chi-square distribution[5] for modeling the distribution of $\left|Y^{(m)}(k)\right|^2$ along with (27) and (28), the probability of false alarm and probability of detection (PD) that will be observed in the presence of ICI and using the threshold as in (40) is given by

$$\begin{aligned}P_{\rm fa,ICI}(P_{\rm fa}) &= \frac{1}{N - \sum_{i=1}^{N_{\rm u}} N_i} \\ &\quad\times \sum_{\substack{k=1,\ldots,N, k\notin\mathbf{\Gamma}_i, \\ i\in\{1,\ldots,N_{\rm u}\}}} Q_M\left(\frac{\sqrt{\tilde{\mu}(k)}}{\tilde{\sigma}(k)}, \frac{\sqrt{\mathrm{F}_Y^{-1}\big(1-\mathrm{P}_{\rm fa}\big)}}{\tilde{\sigma}(k)}\right),\end{aligned} \tag{44}$$

$$\begin{aligned}P_{\rm d,ICI}(P_{\rm fa}) &= \frac{1}{\sum_{i=1}^{N_{\rm u}} N_i} \\ &\quad\times \sum_{\substack{k\in\mathbf{\Gamma}_i, \\ i\in\{1,\ldots,N_{\rm u}\}}} Q_M\left(\frac{\sqrt{\tilde{\mu}(k)}}{\tilde{\sigma}(k)}, \frac{\sqrt{\mathrm{F}_Y^{-1}\big(1-\mathrm{P}_{\rm fa}\big)}}{\tilde{\sigma}(k)}\right),\end{aligned} \tag{45}$$

where from the mean and variance of a non-centralized Chi-square distributed random variable, we may easily obtain

$$\tilde{\mu}(k) = \mathrm{E}\left\{\left|Y^{(m)}(k)\right|^2\right\} - \frac{n_{\rm d}\mathrm{Var}\left\{\left|Y^{(m)}(k)\right|^2\right\}}{4\mathrm{E}\left\{\left|Y^{(m)}(k)\right|^2\right\}} \ , \tag{46}$$

$$\tilde{\sigma}^2(k) = \frac{\mathrm{Var}\left\{\left|Y^{(m)}(k)\right|^2\right\}}{4\mathrm{E}\left\{\left|Y^{(m)}(k)\right|^2\right\}} \ . \tag{47}$$

B. Normalized threshold

Note that NBT discussed in the previous section does not take the received energies of the useful signals into account and selects the threshold based on the noise level. A different way of setting the threshold, which considers both noise and signal energy levels, is to utilize a normalized threshold as follows

$$\xi = P_{\rm n} + T_{\rm norm}\big(P_{\rm s+n} - P_{\rm n}\big) \ , \tag{48}$$

where $P_{\rm n}$ and $P_{\rm s+n}$ are the average noise energy and average signal+noise energy, respectively, and $0 \le T_{\rm norm} \le 1$ denotes the normalized threshold. $P_{\rm n}$ can practically be estimated utilizing the guard bands (GB) of the OFDMA signal. To be more specific, by averaging the energies measured over the outermost subcarriers of left and right GBs, an estimate that is affected least from the ICI can be obtained. $P_{\rm s+n}$, on the other hand, can be roughly determined by averaging the energies measured over all subcarriers except the null subcarriers in the guard bands.

[5]In Section VII-B, it will be verified thorough simulations that Chi-square distribution still well models $\left|Y^{(m)}(k)\right|^2$ in the presence of ICI.

There is a trade-off between probability of false alarms and probability of missed detections in the selection of $T_{\rm norm}$. A too small $T_{\rm norm}$ causes many unused subcarriers to be detected as occupied and gives rise to a high PFA, whereas a too large $T_{\rm norm}$ causes PMD to increase. An analysis of the error probability with respect to the $T_{\rm norm}$ employed is provided in Section VII.

VI. Determining the Optimum Synchronization Point

Depending on its location relative to the primary receiver, a secondary receiver may receive UL-OFDMA signals with $(D_{1,i}-\theta) > N_{\rm CP}$ for certain users, where θ denotes the synchronization point. Interference caused by these users may be significant, especially if the received powers of these users are comparable to users whose $(D_{1,i}-\theta) \le N_{\rm CP}$. This can be the case if the transmit powers of users are unequal, for example due to adaptive power allocation. In a scenario where received powers from all users are similar regardless of d_i, significant interference may be observed.

To have as many spectrum opportunities as possible, the opportunistic system has to minimize the interference that is caused by the timing mismatch. As a solution, the synchronization point can be determined according to $D_{1,i}$ of uplink users; θ may be shifted towards a later point than the intuitive synchronization point, which is the delay of the first arriving user. In practice, user location information (e.g. through GPS) might be utilized by the secondary system to estimate the $D_{1,i}$. In the following, a closed form equation for the interference minimizing synchronization point is derived, denoted by $\theta_{\rm opt}$. As in Section IV-A, the derivation is based on ICI only.

Let $\mathcal{S}$ denote the point where the useful part of the received signal starts, i.e., $\mathcal{S} = \theta + N_{\rm cp}$. Assuming a single occupied subcarrier[6] p_i from each user, and replacing the $N_{\rm cp}$ term in $h_i^2(p,k)$ given in (26) with $\mathcal{S}$, the total ICI power is given by

$$\sum_{k\neq p_i} I_{2,i}^2(k) = \sum_{i=1}^{N_{\rm u}} \sum_{k\neq p_i} \frac{1-\cos\Big(\frac{2\pi(p_i-k)}{N}(D_{1,i}-\mathcal{S})\Big)}{1-\cos\Big(\frac{2\pi(p_i-k)}{N}\Big)} \ , \tag{49}$$

where it is assumed that the $E_{{\rm sc},i}$ and N_i parameters are the same for all users. Differentiating (49) with respect to $\mathcal{S}$ and equating it to 0, we have

$$\frac{d\sum_{k\neq p_i} I_{2,i}^2(k)}{d\mathcal{S}} = \sum_{i=1}^{N_{\rm u}} \sum_{k\neq p_i} \frac{\sin\Big(\frac{2\pi(p_i-k)}{N}(D_{1,i}-\mathcal{S})\Big)}{\cos\Big(\frac{2\pi(p_i-k)}{N}\Big)-1} \frac{2\pi(p_i-k)}{N} = 0 \ . \tag{50}$$

Substituting the cosine and sine terms with the first two terms of their Taylor series expansion, where $p_i - a < k < p_i + a$ as explained in Section IV-A, we obtain

$$\sum_{i=1}^{N_{\rm u}} \sum_{\substack{k=p_i-a \\ k\neq p_i}}^{k=p_i+a} \frac{\frac{2\pi(p_i-k)}{N}(D_{1,i}-\mathcal{S}) - \frac{1}{3!}\Big(\frac{2\pi(p_i-k)}{N}(D_{1,i}-\mathcal{S})\Big)^3}{-\frac{1}{2}\Big(\frac{2\pi(p_i-k)}{N}\Big)^2} \times \frac{2\pi(p_i-k)}{N} = 0 \ , \tag{51}$$

which, after some manipulations, yields

$$\sum_{i=1}^{N_{\rm u}} \sum_{\substack{k=p_i-a \\ k\neq p_i}}^{k=p_i+a} \Big(-2(D_{1,i}-\mathcal{S}) + \Big(\frac{2\pi(p_i-k)}{N}\Big)^2 \frac{(D_{1,i}-\mathcal{S})^3}{3} \Big) \tag{52}$$

$$= \sum_{i=1}^{N_{\rm u}} -4a(D_{1,i}-\mathcal{S}) + \sum_{i=1}^{N_{\rm u}} \Big(\frac{2\pi}{N}\Big)^2 \frac{(D_{1,i}-\mathcal{S})^3}{3} \frac{a(a+1)(2a+1)}{3} \tag{53}$$

$$= \sum_{i=1}^{N_{\rm u}} -(D_{1,i}-\mathcal{S}) + R(D_{1,i}-\mathcal{S})^3 = 0 \ , \tag{54}$$

where $R = \frac{1}{36}\big(\frac{2\pi}{N}\big)^2(a+1)(2a+1)$. Ordering the terms in (54) according to the powers of $\mathcal{S}$, a third order polynomial for $\mathcal{S}$ can be written as

$$N_{\rm u}\mathcal{S}^3 - 3\sum_{i=1}^{N_{\rm u}} D_{1,i}\mathcal{S}^2 + \Big(-\frac{N_{\rm u}}{R} + 3\sum_{i=1}^{N_{\rm u}} D_{1,i}^2\Big)\mathcal{S} - \sum_{i=1}^{N_{\rm u}} D_{1,i}^3 + \frac{1}{R}\sum_{i=1}^{N_{\rm u}} D_{1,i} = 0 \ , \tag{55}$$

The only real root of (55) is $\mathcal{S}_{\rm opt}$, and the optimum synchronization point can be found as $\theta_{\rm opt} = \mathcal{S}_{\rm opt} - N_{\rm cp}$.

A critical point is that if there is a set of users $\mathcal{I}_u$ whose $D_{1,i} < \theta_{\rm opt}$, then the $D_{1,i}$ term in (55) needs to be replaced by $D_{1,i} - \theta_{\rm opt}$ for $i \in \mathcal{I}_u$, and $\mathcal{S}_{\rm opt}$ needs to be recalculated. This is because for $i \in \mathcal{I}_u$, the received symbol contains samples from the previous symbol, and hence, ICI and ISI occur. Therefore, if $\mathcal{I}_u \neq \emptyset$, it is required to run (55) a second time with $D_{1,i}$ modified for $i \in \mathcal{I}_u$ to obtain the correct $\mathcal{S}$. In Section VII, the analytical value of $\theta_{\rm opt}$ obtained from (55) will be verified with computer simulations.

VII. Simulation Results

Extensive computer simulations are performed in order to verify the discussions in the previous sections. In the simulations, both an AWGN channel and a realistic 6-tap multipath (MP) channel (ITU-R Vehicular A channel model) are considered. Signal-to-noise-ratio (SNR) for user i is defined as $\mathrm{E}\{E_{{\rm sc},i}\}/N_0$. PMD is defined as the ratio of number of subcarriers detected as unused although they are used to N. PFA, on the other hand, is the ratio of the number of subcarriers detected as used although they are unused to N. We consider a traffic model where the primary users are continuously transmitting. It is assumed that the scheduling decisions in the primary network remain the same for a certain period

[6]Note that extension to analysis of interference caused by multiple subcarriers follows straight-forwardly through including their effects in the summation below.

of time. The secondary networks sense the spectrum within a portion of this duration and utilize the spectrum opportunities before the scheduling decisions in the primary network change. The simulations target the opportunity sensing aspects of the spectrum, but how the opportunities are utilized is out of the scope of this paper.

A. Statistics of (17) with Timing Misalignment

The mean and variance of (13) for a three user scenario are plotted in Fig. 3, where an AWGN channel is considered. It is observed that theoretical results match well with simulations. While user-1's signal arrives at the receiver with a delay smaller than the CP, user-2 and user-3's signals arrive at the receiver with delays larger than the CP. Fig. 3 shows that the mean and variance of the decision variable $\left|Y^{(m)}(k)\right|^2$ in unoccupied subcarriers adjacent to the subcarriers of user-2 and user-3 are larger than the noise level due to the timing misalignment problem, which will increase the PFA. Another important observation in Fig. 3 is that the variance of the decision variable at the occupied subcarriers of a certain user may increase considerably with the delay experienced by that user, which will impact the probability of detection of the occupied subcarriers. How these factors affect the ROCs will be demonstrated in the next section.

B. Receiver Operating Characteristics With and Without ICI

The ROCs for the three-user scenario in Fig. 3 are illustrated in Fig. 4 for two different SNR levels. Both theoretical and simulation results are shown for NBT, while only simulation results are included for NT with $T_{\text{norm}} \in \{0.2, 0.6\}$. For theoretical NBT, (43) is used when all the users' delays are within the CP (no ICI), while (44) and (45) are used if any of the users' delays are larger than the CP (with ICI). The theoretical plots are well aligned with the simulation results, and it is seen that the Chi-square distribution well models the distribution of $\left|Y^{(m)}(k)\right|^2$ with or without ICI. For NBT, when the propagation delay experienced by the users exceeds the CP, the PD corresponding to a certain PFA decrease for all scenarios due to ICI.

When the NTs are used, on the other hand, the thresholds are not specifically obtained based on the PFA values (captured by the x-axis on the plots), but they are set adaptively based on (48). Then, the simulation results are averaged over several realizations in order to obtain the average PFA and PD values for a given normalized threshold, which are plotted in Fig. 4. It is observed that when the NT in (48) is used, the receiver operates somewhere on the corresponding ROC curves (PD versus PFA relation captured by equations (43)-(45)) at the same SNR. Note that for larger received signal energies, the threshold ξ increases when an NT is used (i.e., the threshold is set adaptively), while it is constant for NBT. Hence, by using NT, the PFA may be decreased with some acceptable degradation in the PD. For example, for $E_{\text{sc},i}/\sigma^2 = 7$ dB and $T_{\text{norm}} = 0.6$ (with no ICI), we have (PFA, PD) $\approx (0.140, 0.920)$ for NT. When the $E_{\text{sc},i}/\sigma^2$ is increased[7] to

[7]Noise level is kept constant and received signal energies are increased.

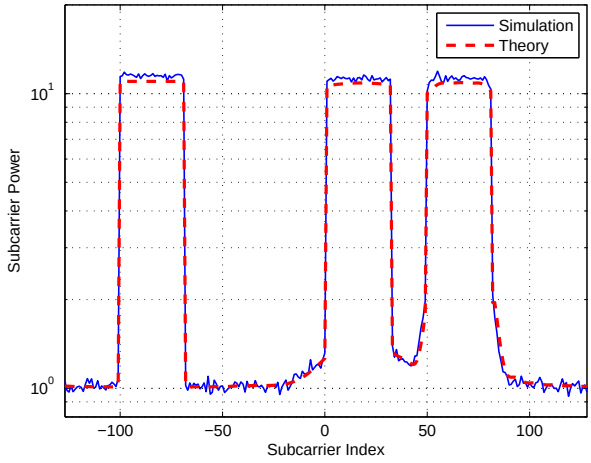

(a) Theoretical versus simulated mean of (17) with timing misalignment.

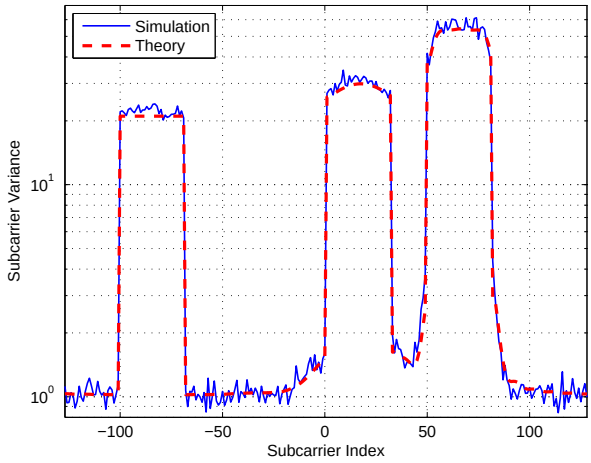

(b) Theoretical versus simulated variance of (17) with timing misalignment.

Fig. 3. Mean and variance of (17) for $E_{\text{sc},i}/\sigma^2 = 10$ dB. User delays in terms of samples are $\tilde{\delta}_1 = 10, \tilde{\delta}_2 = 40$, and $\tilde{\delta}_3 = 60$, while the CP length is equal to 32 samples. Subcarriers assigned to users are $\mathbf{\Gamma}_1 = [-100, -99, ..., -69], \mathbf{\Gamma}_2 = [1, 2, ..., 32], \mathbf{\Gamma}_3 = [50, 51, ..., 81]$, respectively.

10 dB, with NT, the (PFA, PD) $\approx (0.040, 0.983)$. On the other hand, with NBT that uses the same threshold as in the first case, we would have (PFA, PD) $\approx (0.140, 0.993)$, where 0.993 is only slightly larger than 0.983, but 0.040 is considerably smaller compared to 0.140. Hence, through using an NT, considerable improvement may be obtained in the PFA with some minor PD degradation.

C. Probability of Opportunity Detection Error with Timing Misalignment

In this section, two different subcarrier assignment schemes (SAS) are considered. The first one is a blockwise assignment (BA), where each block is defined by N_{symb} consecutive OFDMA symbols and N_{sc} consecutive subcarriers. Fig. 5

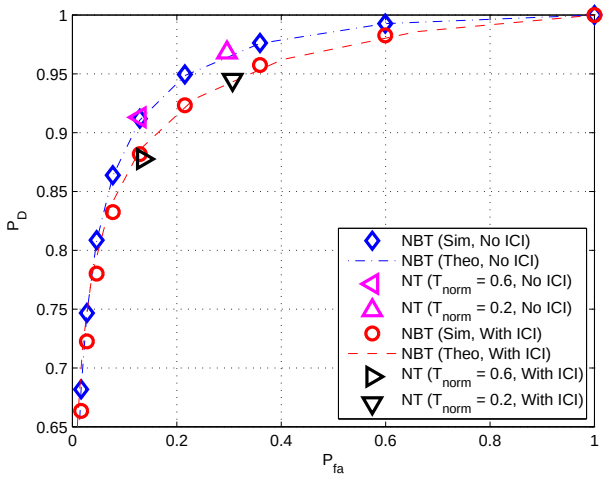

(a) ROCs for $E_{\mathrm{sc},i}/\sigma^2 = 7$ dB.

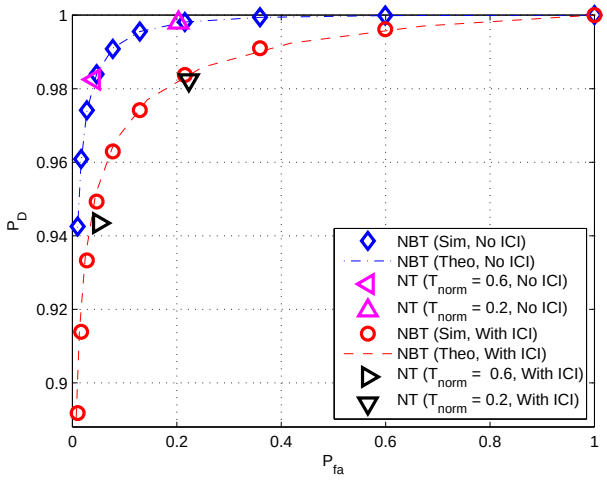

(b) ROCs for $E_{\mathrm{sc},i}/\sigma^2 = 10$ dB.

Fig. 4. Theoretical and simulated ROCs with and without timing misalignment for the three-user scenario in Fig. 3.

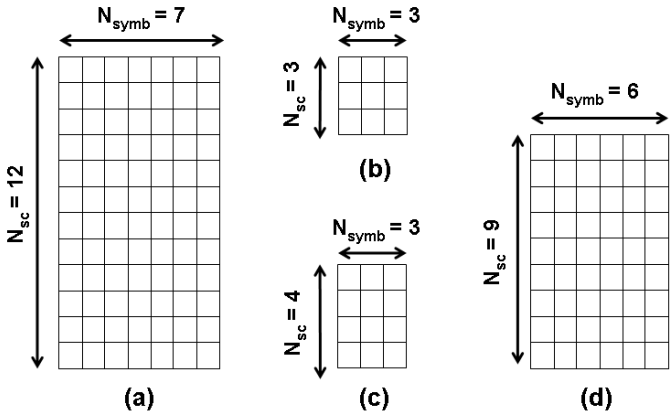

Fig. 5. Subcarrier assignment schemes in different standards. (a) A typical resource block in LTE, (b) PUSC 1 in WiMAX, (c) PUSC 2 in WiMAX, (d) ASP in WiMAX. For the ASP mode in WiMAX, different options for the block dimensions exist, where $N_{\mathrm{symb}} \in \{1, 2, 3, 6\}$ and $N_{sc} = 54/N_{\mathrm{symb}}$ (i.e., number of subcarriers per block is fixed to 54).

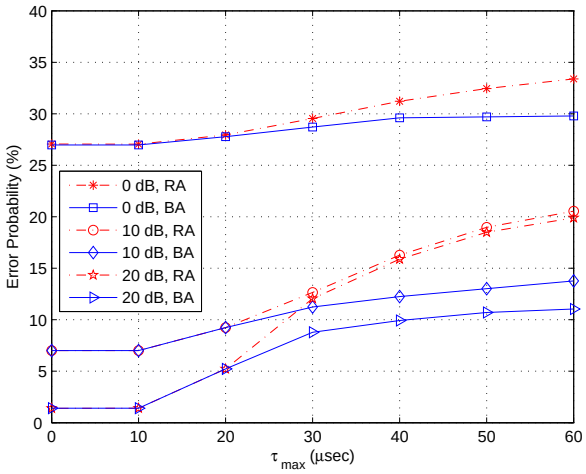

Fig. 6. Error probability versus $\tau_{\max}$ for energy detection with blockwise and randomized assignments ($N_{\mathrm{sc}} = 9, N_{\mathrm{symb}} = 6$).

illustrates the blocks that are used in different standards[8]. The two BA schemes used in the simulations are WiMAX UL ASP with $N_{\mathrm{sc}} = 9$ and $N_{\mathrm{symb}} = 6$, and WiMAX UL PUSC with $N_{\mathrm{sc}} = 4$ and $N_{\mathrm{symb}} = 3$. The other SAS considered is a randomized assignment (RA), where each individual subcarrier may be assigned to a different user. The RA scheme employed in the simulations has $N_{\mathrm{sc}} = 1$ and $N_{\mathrm{symb}} = 6$.

In the simulations, error probability in opportunity detection is computed as the sum of PMD and PFA. For all assignment schemes used, the occupancy rate of the subcarriers is kept at 50% to have equal contribution from PMD and PFA to the total error probability. The maximum delay that the latest arriving user signal can have is $\tau_{\max}$ is considered to be between 0 μs and 60 μs, where $\tilde{\tau}_i \sim \mathcal{U}(0, \tau_{\max})$ for all users. Note that $\tau_{\max}$ values greater than 11.2 μs exceed the CP duration.

Fig. 6 and Fig. 7 demonstrate the error probability for $\tau_{\max}$ values up to 60 μs both for RA and BA, for block sizes 4×3 and 9×6 (shown in Fig. 5(c) and Fig. 5(d)), respectively. The reason for excluding the simulation results for block sizes given in Fig. 5(a) and Fig. 5(b) is their numerical closeness to the other two. Both in Fig. 6 and in Fig. 7, an optimum T_{norm} is used in all cases (see [19] for a detailed analysis of obtaining optimum T_{norm} in different scenarios). It is observed that in RA, ICI has a more destructive effect on the detection performance. The two reasons for the error rates being higher in Fig. 7 than in Fig. 6 are that N_{sc} is smaller leading to a higher number of affected empty subcarriers, and N_{symb} is smaller resulting in worse noise averaging.

The results of the error probability versus $\tau_{\max}$ analysis performed for the ESPRIT algorithm (for a block size of 9×6) are displayed in Fig. 8. It is observed that there is a considerable performance difference between RA and BA in high SNR values. For low SNR, ESPRIT performance is considerably poor regardless of the subcarrier assignment scheme or the $\tau_{\max}$ value. A comparison of the error probabilities

[8]PUSC: partial usage of subchannels, ASP: adjacent subcarrier permutation.

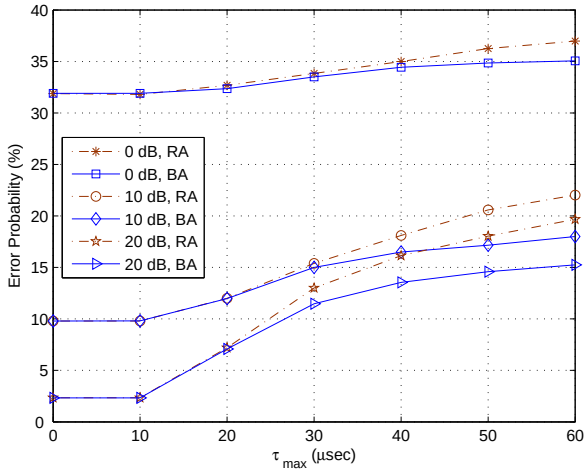

Fig. 7. Error probability versus $\tau_{\max}$ for energy detection with blockwise and randomized assignments ($N_{\rm sc} = 4, N_{\rm symb} = 3$).

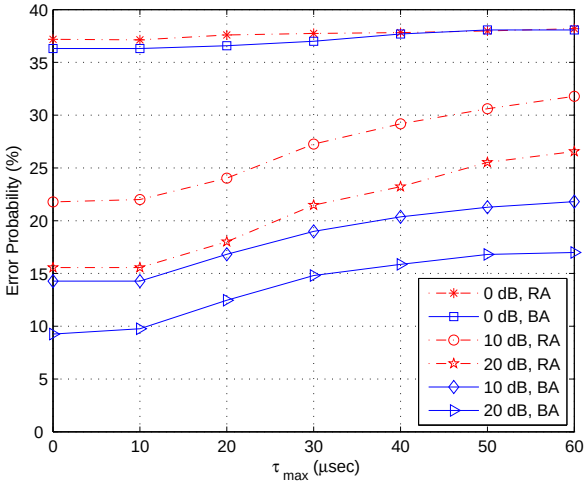

Fig. 8. Error probability versus $\tau_{\max}$ for the ESPRIT algorithm with blockwise and randomized assignments ($N_{\rm sc} = 9, N_{\rm symb} = 6$).

demonstrated in Fig. 6 and Fig. 8 indicates that the ESPRIT performance is inferior to the energy detection performance with the given set of simulation parameters. The main reason for this fact is that there are only 6 symbols over which the ESPRIT algorithm needs to obtain the covariance matrices it requires. It is found that ESPRIT performance could compete with energy detection only if the same subcarrier assignment were used over a very high number of symbols, so that ESPRIT can compute the covariances reliably. The simulation results that compare the performances of these two algorithms up to 500 symbols for RA[9], 20 dB SNR, and $\tau_{\max} = 0$ μs are plotted in Fig. 9. The energy detection curves are obtained for the optimum $T_{\rm norm}$ value for this scenario, which is 0.05, as well as two other non-optimum values. It is shown that

[9]Note that actually there is a sensing vs. throughput trade-off in cognitive radio networks, where there exists an optimal sensing time that maximizes the throughput. Due to space limitations, the reader is referred to [6] for further details.

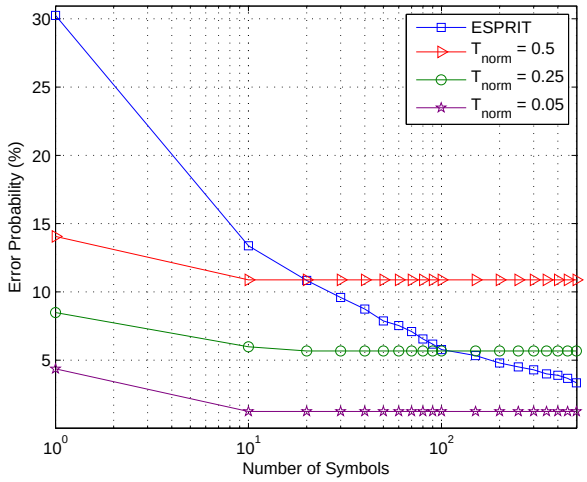

Fig. 9. Comparison of ESPRIT and energy detection algorithms over increasing number of symbols. $T_{\rm norm}$ values considered for energy detection are 0.50, 0.25, and 0.05.

ESPRIT can outperform energy detection at a high number of symbols, especially when $T_{\rm norm}$ is not optimized. However, it is worth to note that ESPRIT becomes less desirable at higher number of symbols due to its increased computational complexity.

Another analysis is performed on the variation of the error probability with respect to $T_{\rm norm}$ in order to determine the optimum $T_{\rm norm}$ in different practical scenarios. In the corresponding simulations, received user signal powers are distance-dependent due to the path loss. It is aimed to detect subcarriers of users whose average SNR exceeds 5 dB. Fig. 10 shows the error probabilities obtained for BA (block size 9×6), where the distances of 12 users to the secondary receiver are shown in the legend. An important observation in Fig. 10 is that the optimum $T_{\rm norm}$ is found to be around 0.05 in all practical scenarios considered.

The variation of interference power with respect to user delay is investigated in Fig. 11 for both AWGN and MP channels. The delays considered are round trip delays (RTDs), and user signal powers are distance-dependent. Theoretical values for interference power are computed using (26), as well, and they validate the simulation results. Note that for the MP channel, interference power is usually higher, and interference is observed even for delays shorter than $N_{\rm cp}$ due to the dispersiveness of the channel. In Fig. 11, the delays yielding the highest interference power that are calculated using (37) are also indicated. It is observed that (37) provides very accurate estimates.

Simulation results for the variation of interference power with respect to the synchronization point (θ) are provided in Fig. 12 for case 1, where user distances vary from 150 m to 1800 m (in steps of 150 m), and for case 2, where user distances vary from 500 m to 1600 m (in steps of 100 m). In both cases, all user signal powers are equal. Theoretical values are also obtained using (49) and they are shown to match with the simulation results. It is revealed that the point where the interference is minimized ($\theta_{\rm opt}$) may be considerably later than

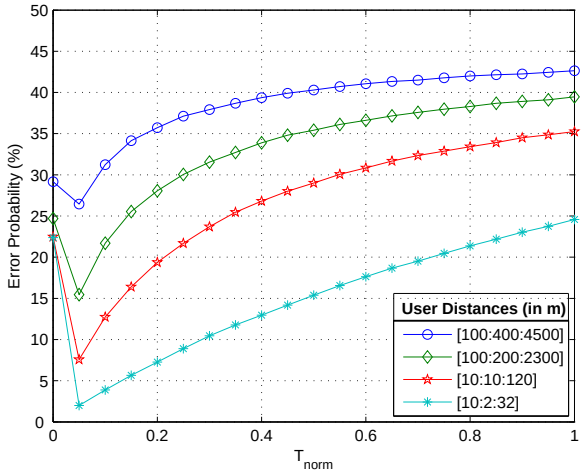

Fig. 10. Error probability versus normalized threshold for 4 different practical scenarios.

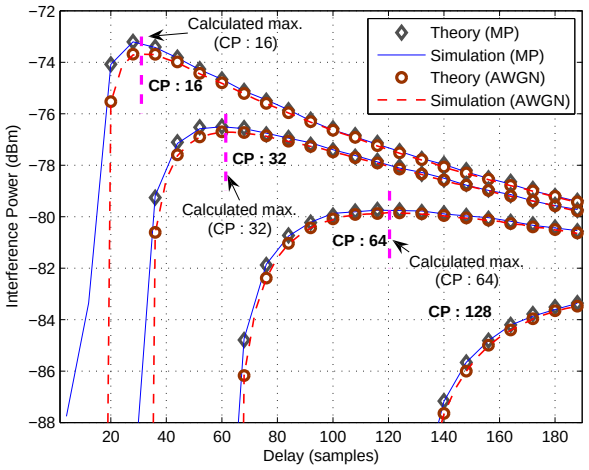

Fig. 11. Interference versus user delay analysis.

the delay of the first arriving signal, and the gain that can be obtained by optimizing the synchronization point may be as high as 3 dB. In Fig. 12, the $\theta_{\rm opt}$ values derived using (55) are indicated, as well. It is observed that (55) is rather accurate in estimating $\theta_{\rm opt}$.

VIII. Concluding Remarks

In this paper, the feasibility of spectrum opportunity detection in UL-OFDMA in the presence of significant timing misalignments is investigated. Energy detection algorithm is scrutinized through detailed theoretical analyses, which are verified through extensive computer simulations. Statistics of the energy detection decision variable are derived in the presence of ICI effects, and are then utilized to obtain the related ROCs. Performance of the energy detector receiver is found to be acceptable, yielding a better performance than the ESPRIT algorithm under the practical system parameters considered. A closed form expression is obtained for the optimum UL-OFDMA synchronization point that minimizes

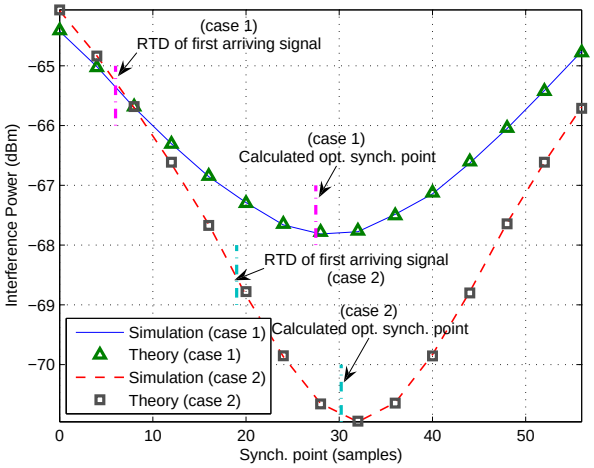

Fig. 12. Variation of ICI power with respect to synchronization point; $N_{\rm CP}$=16 samples. Case 1) User distances (in m): [150:150:1800]. Case 2) User distances (in m): [500:100:1600].

the interference on the cognitive radio. It is shown that it may be at a later point than the arrival time of the earliest primary user's signal.

Appendix

A. Derivation of Energy Detection Statistics for Different Modulations

When BPSK modulation is used, based on (18)-(26), the mean of $\left|Y_i^{(m)}(k)\right|^2$ can be evaluated as follows

$$\mathrm{E}\Big\{\left|Y_i^{(m)}(k)\right|^2\Big\} = \begin{cases} E_{{\rm sc},i}\mathrm{E}\big\{I_{2,i}^2(k)\big\}, & \text{if } k \notin \mathbf{\Gamma}_i, \\ E_{{\rm sc},i}\Big(\mathrm{E}\big\{S_{{\rm d},i}^2(k)\big\} + \mathrm{E}\big\{I_{1,i}^2(k)\big\} + \mathrm{E}\big\{I_{2,i}^2(k)\big\}\Big), & \text{if } k \in \mathbf{\Gamma}_i, \end{cases} \tag{56}$$

where,

$$\mathrm{E}\Big\{S_{{\rm d},i}^2(k)\Big\} = K_{1,i}^2(k)\ , \quad \mathrm{E}\Big\{I_{1,i}^2(k)\Big\} = K_{2,i}^2(k)\ ,$$
$$\mathrm{E}\Big\{I_{2,i}^2(k)\Big\} = \frac{2}{N^2}\sum_{p\in\mathbf{\Gamma}_i, p\neq k} h_i^2(p,k)\ . \tag{57}$$

On the other hand, again based on (18)-(26) (note that (19), (20) are zero-variance RVs), the variance of $\left|Y_i^{(m)}(k)\right|^2$ can be evaluated as

$$\mathrm{Var}\Big\{\left|Y_i^{(m)}(k)\right|^2\Big\} = \begin{cases} E_{{\rm sc},i}^2\mathrm{Var}\big\{I_{2,i}^2(k)\big\}\ , & \text{if } k \notin \mathbf{\Gamma}_i \\ E_{{\rm sc},i}^2\Big(\mathrm{Var}\big\{I_{2,i}^2(k)\big\} + 4\mathrm{Var}\Big\{\mathrm{Re}\big\{S_{{\rm d},i}^*(k)I_{1,i}(k)\big\}\Big\} \\ +4\mathrm{Var}\Big\{\mathrm{Re}\big\{S_{{\rm d},i}^*(k)I_{2,i}(k)\big\}\Big\} + 4\mathrm{Var}\Big\{\mathrm{Re}\big\{I_{1,i}^*(k)I_{2,i}(k)\big\}\Big\}\Big), \\ \text{if } k \in \mathbf{\Gamma}_i, \end{cases} \tag{58}$$

where

$$\mathrm{Var}\{I_{2,i}^2(k)\} = \frac{4}{N^4}\Bigg(\sum_{\substack{p\in\mathbf{\Gamma}_i\\ p\neq k}} h_i^4(p,k) + 4\sum_{\substack{p\in\mathbf{\Gamma}_i\\ p\neq k}}\sum_{\substack{q\in\mathbf{\Gamma}_i\\ q\neq k, q\neq p}} h_i^2(p,k)h_i^2(q,k)\Bigg), \tag{59}$$

$$\mathrm{Var}\Big\{\mathrm{Re}\big\{S_{\mathrm{d},i}^*(k)I_{1,i}(k)\big\}\Big\} = K_{1,i}^2(k)K_{2,i}^2(k) \tag{60}$$

$$\mathrm{Var}\Big\{\mathrm{Re}\big\{S_{\mathrm{d},i}^*(k)I_{2,i}(k)\big\}\Big\} = \frac{1}{N^2}K_{1,i}^2(k)\sum_{p\in\mathbf{\Gamma}_i, p\neq k} h_i^2(p,k)\ , \tag{61}$$

$$\mathrm{Var}\Big\{\mathrm{Re}\big\{I_{1,i}^*(k)I_{2,i}(k)\big\}\Big\} = \frac{1}{N^2}K_{2,i}^2(k)\sum_{p\in\mathbf{\Gamma}_i, p\neq k} h_i^2(p,k)\ . \tag{62}$$

Similar analysis can be applied to higher-order modulation schemes that have symmetric constellation points with respect to the origin, namely the QPSK, 16-QAM, and 64-QAM, where the constellations are respectively given by

$$\mathcal{M}^{(QPSK)} = \Big\{\frac{[(2\rho-1)+(2\kappa-1)j]\sqrt{E_{\mathrm{sc},i}}}{\sqrt{2}}\ , \quad \rho=0,1;\ \kappa=0,1\Big\}, \tag{63}$$

$$\mathcal{M}^{(16-QAM)} = \Big\{\frac{[(2\rho-3)+(2\kappa-3)j]\sqrt{E_{\mathrm{sc},i}}}{\sqrt{10}}\ , \quad \rho=0,1,2,3;\ \kappa=0,1,2,3\Big\}, \tag{64}$$

$$\mathcal{M}^{(64-QAM)} = \Big\{\frac{[(2\rho-7)+(2\kappa-7)j]\sqrt{E_{\mathrm{sc},i}}}{\sqrt{42}}\ , \quad \rho=0,...,7;\ \kappa=0,...,7\Big\}. \tag{65}$$

Then, using (18)-(26), it can easily be derived that the mean and the variance of $\left|Y_i^{(m)}(k)\right|^2$ are identical with (56) and (58) for all the above three constellations of higher-order modulation schemes. Hence, the impact of ICI is independent of the modulation order for constellations that are symmetric with respect to the origin[10].

B. Statistics of (17) in Multipath Channel

In a multipath channel, despite some analogies with with the multiuser channel, the statistics of (17) will be different than in an AWGN channel. We may re-write (17) in a multipath channel as

$$\begin{aligned} P^{(m)}(k) &= \left|Y^{(m)}(k)\right|^2 = \left|Y_i^{(m)}(k)+W(k)\right|^2\ , \\ &= \Bigg|\sqrt{E_{\mathrm{sc},i}}\sum_{l=0}^{L-1}\alpha_i^{(m)}(l) \\ &\quad \Big\{S_{\mathrm{d},i,l}(k)+I_{1,i,l}(k)+I_{2,i,l}(k)\Big\}+W(k)\Bigg|^2, \end{aligned} \tag{66}$$

where a single-user scenario is considered for analytical tractability. After some manipulation, (66) can be written as in (67), where other than the last set of terms involving C_{l_1,l_2}, the earlier terms are analogous to the first three terms in (17) for the multiuser AWGN channel scenario (i.e., the different MPCs in the multipath channel may be considered as multiuser signals with different delays and attenuations), and their statistics have already been captured through equations (18)-(30). However, as opposed to the multiuser AWGN channel scenario analogy, the C_{l_1,l_2} term will be non-zero in the multipath channel, since the MPCs corresponding to the same user will be using the same SAS as well as the same modulated symbols (as opposed to the last term in (17)). The term C_{l_1,l_2} can be expanded for the multipath channel as

$$\begin{aligned} &\big(S_{\mathrm{d},i,l_1}(k)+I_{1,i,l_1}(k)+I_{2,i,l_1}(k)\big) \\ &\qquad\times\big(S_{\mathrm{d},i,l_2}(k)+I_{1,i,l_2}(k)+I_{2,i,l_2}(k)\big) \\ &= S_{\mathrm{d},i,l_1}(k)S_{\mathrm{d},i,l_2}(k)+S_{\mathrm{d},i,l_1}(k)I_{1,i,l_2}(k) \\ &+ S_{\mathrm{d},i,l_1}(k)I_{2,i,l_2}(k)+I_{1,i,l_1}(k)S_{\mathrm{d},i,l_2}(k)+I_{1,i,l_1}(k)I_{1,i,l_2}(k) \\ &+ I_{1,i,l_1}(k)I_{2,i,l_2}(k)+I_{2,i,l_1}(k)S_{\mathrm{d},i,l_2}(k)+I_{2,i,l_1}(k)I_{1,i,l_2}(k) \\ &+ I_{2,i,l_1}(k)I_{2,i,l_2}(k)\ . \end{aligned} \tag{68}$$

In (68), only the $S_{\mathrm{d},i,l_1}(k)S_{\mathrm{d},i,l_2}(k)$, $I_{1,i,l_1}(k)I_{1,i,l_2}(k)$, and $I_{2,i,l_1}(k)I_{2,i,l_2}(k)$ terms have a non-zero mean. For example, the first term is equal to

$$\begin{aligned} &S_{\mathrm{d},i,l_1}(k)S_{\mathrm{d},i,l_2}(k) \\ &= \big[X_i^{(m)}(k)\big]^2K_{1,i,l_1}(k)K_{1,i,l_2}(k)e^{\frac{-j2\pi k(D_{l_1,i}+D_{l_2,i})}{N}}. \end{aligned} \tag{69}$$

If $D_{l_1,i}$ and $D_{l_2,i}$ are considered as known, (69) becomes a deterministic variable[11]. Similarly, it may be shown that the other two terms have non-zero means, and it is also straightforward to derive that (68) has a non-zero variance. In summary, since the C_{l_1,l_2} terms are non-zero in a multipath channel, there is not a one-to-one analogy between single-user multipath and multi-user AWGN channels, and the former scenario (considering exactly same delays and fading coefficients as in a multiuser AWGN channel) results in worse spectrum opportunities due to larger ICI.

ACKNOWLEDGMENT

The authors would like to thank Dr. Moo-Ryong Jeong and Dr. Fujio Watanabe of DOCOMO Communications Labs, USA, for their helpful inputs.

[10]Note that the statistics will change in case different modulation types are used for two consecutive symbols, where one of them is at the end of a certain block and the following symbol is at the beginning of the following block.

[11]If $D_{l_1,i}$ and $D_{l_2,i}$ are considered as random variables that may take any value, on the other hand, the mean of (69) would be equal to zero. However, these two variables usually have small values compared to N, and therefore, (68) still has a non-negligible mean.

$$P^{(m)}(k) = E_{\mathrm{sc},i} \sum_{l=0}^{L-1} \left|\alpha_i^{(m)}(l)\right|^2 \Bigg[\left|S_{\mathrm{d},i,l}(k)\right|^2 + \left|I_{1,i,l}(k)\right|^2 + \left|I_{2,i,l}(k)\right|^2 + 2\mathrm{Re}\Big\{ S^*_{\mathrm{d},i,l}(k) I_{1,i,l}(k) + S^*_{\mathrm{d},i,l}(k) I_{2,i,l}(k) + I^*_{1,i,l}(k) I_{2,i,l}(k) \Big\} \Bigg]$$
$$+ |W(k)|^2 + 2\mathrm{Re}\Bigg\{ W^*(k) \sqrt{E_{\mathrm{sc},i}} \sum_{l=0}^{L-1} \alpha_i^{(m)}(l) \Big\{ S_{\mathrm{d},i,l}(k) + I_{1,i,l}(k) + I_{2,i,l}(k) \Big\} \Bigg\}$$
$$+ 2E_{\mathrm{sc},i} \sum_{l_1=0}^{L-2} \sum_{l_2=l_1+1}^{L-1} \alpha_i^{(m)}(l_1) \alpha_i^{(m)}(l_2) \underbrace{\Big[\big(S_{\mathrm{d},i,l_1}(k) + I_{1,i,l_1}(k) + I_{2,i,l_1}(k)\big) \big(S_{\mathrm{d},i,l_2}(k) + I_{1,i,l_2}(k) + I_{2,i,l_2}(k)\big) \Big]}_{C_{l_1,l_2}}. \tag{67}$$

REFERENCES

[1] S. Haykin, "Cognitive radio: brain-empowered wireless communications," *IEEE J. Sel. Areas Commun. (JSAC)*, vol. 23, no. 2, pp. 201–220, 2005.

[2] G. Ganesan and Y. G. Li, "Cooperative spectrum sensing in cognitive radio, part I: Two user networks," *IEEE Trans. Wireless Commun.*, vol. 6, no. 6, pp. 2204–2213, June 2007.

[3] ——, "Cooperative spectrum sensing in cognitive radio, part II: Multiuser networks," *IEEE Trans. Wireless Commun.*, vol. 6, no. 6, pp. 2214–2222, June 2007.

[4] S. Mangold, Z. Zhong, K. Challapali, and C.-T. Chou, "Spectrum agile radio: radio resource measurements for opportunistic spectrum usage," in *Proc. IEEE Global Telecommun. Conf. (GLOBECOM)*, vol. 6, Dallas, TX, Nov. 2004, pp. 3467–3471.

[5] J. Hillenbrand, T. A. Weiss, and F. K. Jondral, "Calculation of detection and false alarm probabilities in spectrum pooling systems," *IEEE Commun. Lett.*, vol. 9, no. 4, pp. 349–351, Apr. 2005.

[6] Y. C. Liang, Y. Zeng, E. C. Y. Peh, and A. T. Hoang, "Sensing-throughput tradeoff for cognitive radio networks," *IEEE Trans. Wireless Commun.*, vol. 7, no. 4, pp. 1326–1337, Apr. 2008.

[7] J. Ma and Y. G. Li, "Soft combination and detection for cooperative spectrum sensing in cognitive radio networks," in *Proc. IEEE Global Telecommun. Conf. (GLOBECOM)*, Washington, DC, Nov. 2007, pp. 3139–3143.

[8] J.-H. Baek, H.-J. Oh, and S.-H. Hwang, "Improved reliability of spectrum sensing using energy detector in cognitive radio system," in *Proc. Int. Conf. Adv. Commun. Technol. (ICACT)*, vol. 1, Gangwon-Do, Korea, Feb. 2008, pp. 575–578.

[9] M. El-Tanany, Y. Wu, and L. Hazy, "OFDM uplink for interactive broadband wireless: Analysis and simulation in the presence of carrier, clock, and timing errors," *IEEE Trans. Broadcast*, vol. 47, no. 1, pp. 3–19, Mar. 2001.

[10] M. Park, K. Ko, H. Yoo, and D. Hong, "Performance analysis of OFDMA uplink systems with symbol timing misalignment," *IEEE Commun. Lett.*, vol. 7, no. 8, pp. 376–378, Aug. 2003.

[11] E. Bala and L. J. Cimini, "On the uplink synchronization of OFDMA systems," in *Proc. IEEE Military Commun. Conf. (MILCOM)*, Atlantic City, NJ, Oct. 2005, pp. 1133–1139.

[12] L. T. W. Ho and H. Claussen, "Effects of user-deployed, co-channel femtocells on the call drop probability in a residential scenario," in *Proc. IEEE Int. Symp. Personal, Indoor and Mobile Radio Commun. (PIMRC)*, Athens, Greece, Sep. 2007, pp. 1–5.

[13] H. Claussen, "Performance of macro- and co-channel femtocells in a hierarchical cell structure," in *Proc. IEEE Int. Symp. Personal, Indoor and Mobile Radio Commun. (PIMRC)*, Athens, Greece, Sep. 2007, pp. 1–5.

[14] V. Chandrasekhar and J. G. Andrews, "Uplink capacity and interference avoidance for two-tier cellular networks," in *Proc. IEEE Global Telecommun. Conf. (GLOBECOM)*, Washington, DC, Nov. 2007, pp. 3322–3326.

[15] V. Chandrasekhar, J. Andrews, and A. Gatherer, "Femtocell networks: a survey," *IEEE Commun. Mag.*, vol. 46, no. 9, pp. 59–67, September 2008.

[16] H. Mahmoud, H. Arslan, and M. Ozdemir, "Initial Ranging for WiMAX (802.16e) OFDMA," in *Proc. IEEE Military Commun. Conf. (MILCOM)*, Washington, DC, Oct. 2006, pp. 1–7.

[17] Y. Choi, S. Park, and S. Bahk, "Multichannel random access in OFDMA wireless networks," *IEEE J. Sel. Areas Commun. (JSAC)*, vol. 24, no. 3, pp. 603–613, 2006.

[18] I. Guvenc, "Statistics of macrocell-synchronous femtocell-asynchronous users' delays for improved femtocell uplink receiver design," *IEEE Commun. Lett.*, vol. 13, no. 4, pp. 239–241, Apr. 2009.

[19] M. E. Sahin, I. Guvenc, M. R. Jeong, and H. Arslan, "Opportunity detection for OFDMA systems with timing misalignment," in *Proc. IEEE Global Telecommun. Conf. (GLOBECOM)*, New Orleans, LA, Nov. 2008, pp. 1–6.

[20] J. V. Beek, P. O. Borjesson, M. L. Boucheret, D. Landstrom, J. M. Arenas, P. Odling, C. Ostberg, M. Wahlqvist, and S. K. Wilson, "A time and frequency synchronization scheme for multiuser OFDM," *IEEE J. Sel. Areas Commun. (JSAC)*, vol. 17, no. 11, pp. 1900–1914, Nov. 1999.

[21] M. Morelli, "Timing and frequency synchronization for the uplink of an OFDMA system," *IEEE Trans. Commun.*, vol. 52, no. 2, pp. 296–306, Feb. 2004.

[22] R. Roy and T. Kailath, "ESPRIT-estimation of signal parameters via rotational invariance techniques," *IEEE Trans. Acoust., Speech, and Signal Process.*, vol. 37, no. 7, pp. 984–995, Jul. 1989.

[23] B. Ottersten, M. Viberg, and T. Kailath, "Performance analysis of the total least squares ESPRIT algorithm," *IEEE Trans. Signal Process.*, vol. 39, no. 5, pp. 1122–1135, May 1991.

[24] B. Yang, K. Letaief, R. Cheng, and Z. Cao, "Channel estimation for OFDM transmission in multipath fading channels based on parametric channel modeling," *IEEE Trans. Commun.*, vol. 49, no. 3, pp. 467–479, Mar. 2001.

[25] R. Roy, A. Paulraj, and T. Kailath, "ESPRIT– A subspace rotation approach to estimation of parameters of cisoids in noise," *IEEE Trans. Acoust., Speech, and Signal Process.*, vol. 34, no. 5, pp. 1340–1342, Oct. 1986.

[26] U. Tureli, H. Liu, and M. Zoltowski, "OFDM blind carrier offset estimation: ESPRIT," *IEEE Trans. Commun.*, vol. 48, no. 9, pp. 1459–1461, Sep. 2000.

[27] T. Yucek, "Channel, Spectrum, and Waveform Awareness in OFDM-Based Cognitive Radio Systems," Ph.D. dissertation, University of South Florida, 2007.

[28] M. Wax and T. Kailath, "Detection of signals by information theoretic criteria," *IEEE Trans. Acoust., Speech, Signal Process.*, vol. 33, no. 2, pp. 387–392, 1985.

[29] J. G. Proakis, *Digital Communications*, 4th ed. New York: McGraw-Hill, 2001.

Mustafa Emin Şahin received his B.S. degree in Electrical and Electronic Engineering from Boğaziçi University, Istanbul, Turkey, in June 2004, and his M.S. degree in Electrical Engineering from the University of South Florida, Tampa, FL, USA, in May 2006. He is a member of the Wireless Communications and Signal Processing Group at University of South Florida and he is working toward his Ph.D. degree. During his Ph.D. study, he has been collaborating with researchers in DOCOMO USA Communications Laboratories, Palo Alto, CA. His research interests include OFDMA-based co-channel femtocells, co-channel interference cancellation in OFDMA, MIMO implementation in WiMAX systems, and spectrum sensing in cognitive radios.

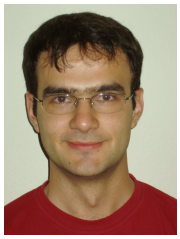

Ismail Guvenc received his B.S. degree from Bilkent University, Turkey, in 2001, M.S. degree from University of New Mexico, Albuquerque, NM, in 2003, and Ph.D. degree from University of South Florida, Tampa, FL, in 2006 (with Outstanding Dissertation Award from USF Graduate School), all in Electrical Engineering. He was with Mitsubishi Electric Research Labs in Cambridge, MA, in 2005. Since June 2006, he has been with DOCOMO USA Labs, Palo Alto, CA, working as a research engineer. His recent research interests include femtocells, LTE systems, cognitive radio, and UWB communications and localization. He has published more than 50 international conference and journal papers, and several standardization contributions for the IEEE 802.15 and IEEE 802.16 standards. Dr. Guvenc has served in the organizing and technical program committees of several international conferences, and co-authored a book on ultrawideband position estimation. He has over 15 pending U.S. patent applications and he is a member of the IEEE.

Dr. Hüseyin Arslan has received his PhD. degree in 1998 from Southern Methodist University (SMU), Dallas, Tx. From January 1998 to August 2002, he was with the research group of Ericsson Inc., NC, USA, where he was involved with several project related to 2G and 3G wireless cellular communication systems. Since August 2002, he has been with the Electrical Engineering Dept. of University of South Florida. In addition, he has worked as part time consultant for various companies and institutions including Anritsu Company, The Scientific and Technological Research Council of Turkey- TUBITAK, Lecroy, and XG technologies.

Dr. Arslan's research interests are related to advanced signal processing techniques at the physical layer, with cross-layer design for networking adaptivity and Quality of Service (QoS) control. He is interested in many forms of wireless technologies including cellular, wireless PAN/LAN/MANs, fixed wireless access, and specialized wireless data networks like wireless sensors networks and wireless telemetry. The current research interests are on UWB, OFDM based wireless technologies with emphasis on WIMAX and IMT-Advanced, and cognitive and software defined radio. He has served as technical program committee chair, technical program committee member, session and symposium organizer, and workshop chair in several IEEE conferences. He is a member of the editorial board for "Wireless Communication and Mobile Computing Journal" and "Research Letters in Communications". Dr. Arslan is a senior member of IEEE.